Journal of Applied Polymer Science

Gel structure phase behavior in micro nanofibrillated cellulose containing *in situ* precipitated calcium carbonate

Katarina Dimic-Misic,[1] Juuso Rantanen,[1] Thad C. Maloney,[1] Patrick A. C. Gane[1,2]
[1]School of Chemical Technology, Department of Forest Products Technology, Aalto University, 00076, Aalto Helsinki, Finland
[2]Omya International AG, Baslerstrasse 42, Oftringen, CH-4665, Switzerland
Correspondence to: K. Dimic-Misic (E-mail: katarina.dimic.misic@aalto.fi)

ABSTRACT: Speciality high-strength board, packaging grades, and novel cellulose-based nanocomposites may incorporate microcellulosic nanofibrillated materials (MNFC), although the rheological properties of such strongly water sorbing structures are challenging for processing technologies. This study introduces rheological methods for the evaluation of dewatering and flow behavior of such high consistency furnishes to exemplify the effect of energy input on microfibrillar material (MFC), as produced by a combination of enzymatic pretreatment and increased levels of fluidization. The large number of fibril contact points act to entrap water, held both on the fibril surface as immobilized water and in the interfibril spacing forming the gel structure. Tuning of the rheological and dewatering properties has been enabled by *in situ* precipitation of calcium carbonate filler (*in situ* PCC) on the MFC, which results in the production of a more uniform furnish. Such *in situ* PCC coated MFC fibrils incorporated into furnish were seen to increase dewatering rate over that of the furnish mix without the *in situ* precipitated filler primarily because of the reduction in total surface area of the fibers and fibrils when the pigment is present on the fibrillary surface. © 2016 Wiley Periodicals, Inc. J. Appl. Polym. Sci. **2016**, *133*, 43486.

KEYWORDS: cellulose and other wood products; composites; gels; rheology; viscosity and viscoelasticity

Received 6 November 2015; accepted 30 January 2016
DOI: 10.1002/app.43486

INTRODUCTION

Sustainability is one of the key targets for industrial practice today, and the research aimed at new materials development based on renewable sources replacing traditional oil-based products is widely considered as highly relevant.[1,2] In the forest products industry nano (NFC) and microfibrillated cellulose (MFC) have attracted attention because of a number of potential applications not only in paper and board manufacturing but also in other industrial value chains, such as nanocomposites.[3–5] Micro nanofibrillated cellulose (MNFC) has interesting intrinsic properties, exhibiting particularly high specific surface area, flexibility, regions of crystallinity, and surface chemistry presenting hydroxyl groups for possible chemical modification.[6–8] Such properties influence their particulate interactions on a colloidal level, especially when combined with other components in complex suspensions, impacting strongly on flow-related processes and dewatering.[9–12]

Mechanical methods of MNFC production use high pressure homogenizers, microfluidic cells, rotor-stators, refiners, and super masscolloider or microgrinders to break up the wood fibers to dimensions of 100–50 nm in diameter.[13–17] Application of chemical methods prior to mechanical treatments, such as enzymatic pretreatment, drastically reduces energy consumption.[18–20] Refining of enzymatically pretreated pulp using a microfluidizer/homogenizer is one novel route in MFC and NFC production designed to reduce problems typically related to clogging of refiner systems,[15,21–23] thus enabling production of higher consistency suspensions by employing the high shear zone through the fluidizer chamber while obtaining the desired higher aspect ratio nano or microscale product via repeated passes.[6,13] Such methods are frequently used to transform microfibrillated material (MFC) into nanofibrillated forms (NFC). Materials lying between these two categories are termed here MNFC. High consistency composite materials consisting of a mixture of traditional pulp fibers and MNFC have attracted much attention in recent years. Such composites are attractive because of the possibility to use reduced amounts of pulp fibers and drastically increased amounts of fillers, enabled via increased hydrogen bonding of high aspect ratio MNFC, which adds to the increase in both optical properties (higher filler loading) and strength (hydrogen bonding) of the final product. Problems arising in practice with such high consistency MNFC furnishes are related mainly to the difficulty in dewatering. Therefore, in order to propose novel processes for their implementation it is necessary to understand their complex dewatering behavior and rheology. The scope of this research includes

utilizing findings related to the influence of the MNFC production route on the agglomeration and colloidal gel-like nature of complex MNFC-filler suspensions, in order to propose ways in which these composite materials can successfully be characterized, classified, and applied.

In this research we contribute further to the rheological evaluation of different grades of MNFC, obtained with enzymatic pretreatment of pulp, by controlling the level of postfluidizing.[6,19,20] This enzymatically pretreated MFC is studied as an additive in high consistency high filler load furnish.[5,6] Of novel importance in this work is the as yet not studied effect on rheology and dewatering of the inclusion of *in situ* calcium carbonate precipitation onto MFC (*in situ* PCC-MFC costructure) when added to fiber furnish.[6] Analysis of the resulting rheological and dewatering properties shows interesting advantageous comparison with non-PCC-costructured MFC, adding easier processing whilst maintaining the superior mechanical properties that were previously published.[6]

MATERIALS AND METHODS

Furnish, MFC, and Fillers

The pulp used for the papermaking furnish was once dried bleached softwood Kraft pulp (BSK), originating from a Finnish pulp mill with a weighted average fiber length of 2.23 mm measured with a FiberLab analyzer (Metso Automation). The freely added filler for comparison was PCC commercial grade Syncarb FS-240 from Omya International AG, Switzerland. It was delivered as a water suspension at 35 wt %, essentially dispersant-free polysaccharide stabilized against sedimentation. Never dried bleached hardwood Kraft pulp from a Finnish pulp mill was used in the MFC preparation process, as described by Rantanen *et al.*[6] The hardwood Kraft pulp was subjected to an enzymatic pretreatment and prerefining in a Valley beater for 30 min in order to facilitate the fibrillation of the fibers. The thus refined enzymatically pretreated sample was used as a reference for the other MFC samples that were subsequently fed through the microfluidizer/homogenizer at 2000 bar through the 100 µm opening (Microfluidizer M-110P supplied by Microfluidics, USA). The solids content of the MFC suspensions was 1.65 wt % after the fluidization. A series of products, employing 1, 2, and 5 passes (1MFC, 2MFC, and 5MFC), respectively, through the microfluidizer/homogenizer, were made to study the effect of nanofibrillation/degree of fibrillation on the MFC surface on swelling and the consequent rheological properties in water suspension.

In Situ Precipitation of Calcium Carbonate on MFC and Furnish Compositions

As a result of the balanced satisfactory quality of product and medium energy consumption of the 2 pass MFC (2MFC), compared with the 5 pass grade (5MFC), it was chosen for the *in situ* calcium carbonate precipitation process. The calcium carbonate (PCC) was precipitated on the surface of the 2MFC, as described by Rantanen *et al.*[6] *In situ* precipitation was made by feeding a mix of the 2MFC and $Ca(OH)_2$ (slaked lime) into a reactor, into which was fed CO_2 gas through the suspension, as presented in Figure 1, to form PCC via the well-known precipitation reaction in water

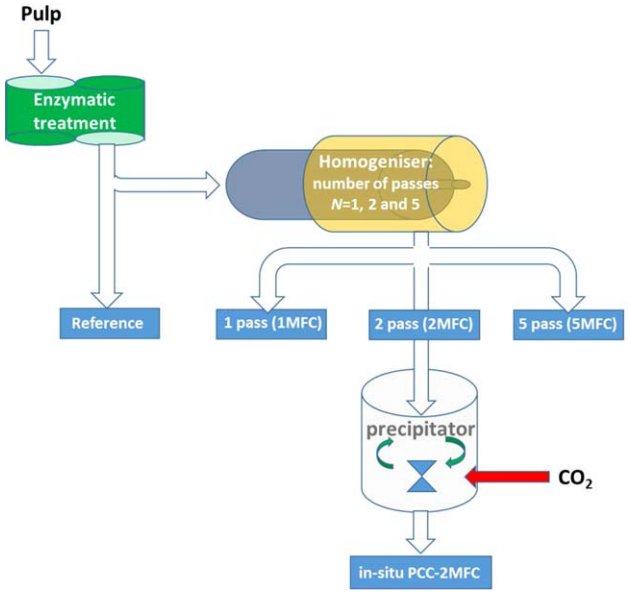

Figure 1. Schematic representation of the MFC enzymatic and homogenizing process, showing the 2 pass grade (2MFC) with further *in situ* precipitation to form the "*in situ* PCC-2MFC" costructure. [Color figure can be viewed in the online issue, which is available at wileyonlinelibrary.com.]

$$CaO + H_2O \rightarrow Ca(OH)_2 \quad : \quad Ca(OH)_2 + CO_2 \rightarrow CaCO_3 + H_2O \tag{1}$$

As a result, PCC nanoparticles were formed on the surface of the 2MFC, creating a PCC-MFC costructure (*in situ* PCC-2MFC). The presence of MNFC and cellulosic moieties during the precipitation will act to modify the PCC crystal growth, and so there will undoubtedly be differences in particle morphology between standard free precipitated carbonate and the *in situ* version. However, this is not considered to be a major factor with respect to the advantages found for *in situ* coprecipitation, since the coprecipitated morphology will necessarily be less well-defined with respect to crystal morphology. This varied morphology would be expected to show less specific packing interaction, and if such a morphological mix was to be added freely would actually deliver the opposite effect in many respects to that found.

Two different precipitation levels on the surface of 2MFC were performed, which resulted in an amount of 10.6 and 75.5 wt %, respectively, of the total dry weight of the filler being precipitated on the 2MFC fibers, measured via the ash content.[6]

The furnishes were made down into two consistencies, 4 and 7 wt % solids content, respectively, with furnish composition being 70% PCC filler in total, either free, in the costructure or both costructure and free combined, 20% MFC product [Ref (prior to homogenizing), 1, 2, and 5 pass homogenized, respectively] and 10% cellulose pulp fibers.[6]

Furnish Mixes

The high level of filler, unusual for paper and board manufacture, is to represent the target of a filler–fiber composite material, which is considered as a realistic sustainable natural

Table I. Furnish Formulations and Labelling, in Accordance with Figure 1

Consistency/%	Furnish formulation pulp fibers (%)/fluidized MFC (%)/ number of homogenizer passes in MFC production (*n*P)/PCC *in situ* (%)/free PCC filler addition (%)	Sample label solids/ MFC type[a]
N = {4, 7}	10/20/Ref/0/70	*N*/Ref
	10/20/1P/0/70	*N*/1P
	10/20/2P/0/70	*N*/2P
	10/20/2P/2.3/67.7	*N*/2P/LOW
	10/20/2P/61.6/8.4	*N*/2P/HIGH
	10/20/5P/0/70	*N*/5P

[a]MFC described by the number of passes, and by amount of *in situ* PCC in the costructure (LOW and HIGH).

polymer composite replacement.[5,6,24] The sample labels follow the notation: consistency/MFC grade/ratio of total pigment precipitated on MFC. The composition ratio of the furnish was constant in all experiments with 70% filler in total, 20% MFC, and 10% pulp fibers, and in the case after the precipitation reactor was the 2 pass MFC coated with PCC (*in situ* PCC-2MFC costructure). In the rheological measurements, the test suspension in each case was at 4 and 7 wt %, as presented in Table I.

Characterization of Materials.

Zeta Potential and Particle Size of Freely Added PCC Filler

To help characterize the constituents, the charge of the freely added filler pigment, defined by the zeta potential, ζ, was determined by a Zeta-sizer (Malvern Instruments). The particle size of the pigment, MNFC and flocculated pigment agglomerates was measured with dynamic light scattering (DLS), using the photon correlation spectroscopic technique on the same instrument. Prior to measuring the ensemble defined particle size, the samples were diluted with de-ionized water to a solid content of 0.01 wt %. The scattering volume equivalent diameter, d_{sv}, and ζ are reported as an average of at least five runs. In the case where the density of a material is constant throughout its size distribution, the volume, and weight determined size distribution are identical.

Scanning Electron Microscopy. For the microstructural analysis of the effect of microfluidization on fibril morphology a field emission scanning electron microscope (FE-SEM, Zeiss Sigma) was used. Prior to freeze drying at −50 °C and 2.4 Pa pressure, the MFC suspensions were filtered on filter paper using a Büchner funnel. The surface of the freeze dried samples was coated with a thin conducting layer of gold and imaged in the high vacuum mode. The accelerating voltage was 2.5 kV.

Gravimetric Dewatering and Gel Network Water Retention

The static gravimetric dewatering of suspensions and furnishes was measured using the Åbo Akademi Gravimetric Water Retention device (ÅA-GWR). A volume of 10 cm^3 of the MFC containing furnish was inserted into the cylindrical vessel above a polycarbonate membrane (Nucleopore Track-Etch membrane 5 μm, Whatman) and sufficient layers of absorbent blotting paper, defined to absorb the subsequent water loss volume in the experiment, and, after closing the cylinder, the sample was held under overpressure of 0.5 bar, as described in detail previously.[24,25]

The network level swelling of MFC and NFC was evaluated with a water retention value test (WRV, ISO/DIS 23714). The WRV test was slightly modified to suit the measurement of the nanocellulosic materials.[5,24,25] This was done by mixing quantities of the nanocellulose in the range 0–6% with an unrefined Kraft pulp and then centrifuging the mixture under normal WRV test conditions. The curve of WRV against nanocellulose content can be used to calculate the pure nanocellulose swelling.[24,25]

RHEOLOGICAL MEASUREMENTS

A rotational and oscillation rheometer (Physica MCR-300) was used in both controlled shear and strain modes with a plate–plate geometry. The rheometer was equipped with roughened (serrated) top (PP20) and bottom (P-PTD 200) plates,[24–26] the bottom plate implementing a Peltier temperature control, with fixed temperature at 23 °C. The gap between plates was initialized to 2.5 mm. The linear viscoelastic region (LVE) was identified with oscillatory measurements applying a strain sweep, at a constant angular frequency (ω) of 0.1 rad.s^{-1}, after which frequency sweep measurements were performed within the LVE where the strain (γ) was varied between 0.01 and 500%. It should be noted here that complex systems, as described by the materials used in this study, i.e. macrofibrous as well as colloidal particulates, undergo multiple structural configurations[10,11] including, and generating, a variety of elastic interactions.[27,28] Thus, the term LVE in this context refers to the particular LVE region applicable for the fixed frequency of oscillation used.[24,29] The influence of shear rate on the variation of dynamic viscosity (η) was observed using the steady state flow curves over the shear rate range of 0.001–1000 s^{-1}.[27,30] Once shear thinning occurs, there is no natural damping or particle collective motion, and so the system becomes highly sensitive to particulate-driven swings in viscosity at overall very low viscosity levels. The noise is assumed random, and in principle could be averaged, but since it occurs well away from the initial thixotropic viscosity drop region of interest, this behavior is considered irrelevant.

With the Tikhonov regularization based smoothing method we obtained suitable rheograms for determining rheological parameters, as described in detail and defined in our previous work,[57] using the following transformations:

$$A\vec{x}=\vec{y} \quad (2)$$

where A is a matrix and $\vec{x}$, $\vec{y}$ vectors. In eq. (1), $\vec{y}$ represents an observed variable, the measurements of which are subjected to some nonsystematic variation or noise, whereas $\vec{x}$ on the other hand is an unmeasured quantity. In Tikhonov regularization the minimization problem

$$\min_x \|A\vec{x}-\vec{y}\|^2 \quad (3)$$

is replaced by the penalized minimization problem

$$\min_x \left\{\|A\vec{x}-\vec{y}\|^2+\lambda\|L\vec{x}\|^2\right\} \quad (4)$$

where L is a matrix termed as the regularization matrix, and λ is a positive parameter. The purpose of the second term in the expression to be minimized is to penalize (suppress) extreme solutions and favor physical ones. Data smoothing is achieved by setting the matrix A in eq. (3) to the identity matrix and selecting the regularization matrix in such a way that it penalizes data fluctuations.

Rheograms were constructed from the representative measurements (after smoothing), while at least five samples were included in the analysis. Data variation of ÅA-GWR was within ± 5%, while for rheometer and dynamic dewatering (IMC) within ± 7–10%, strongly related to the varied nature of the materials spanning the geometry, in particular the particulate size and physical interactions, leading to the likely presence of shear inhomogeneity in the plate–plate geometry contributing to reduced reproducibility, including the potential for wall slip and the glassy low friction state within the suspension.[27,36,37,50,57]

Yield Stress

Yield stress is perhaps the most important rheological property of complex suspensions, as it needs to be exceeded in the order that flow takes place.[31,32] MNFC suspensions are gel-like and exhibit a short range dynamic yield effect.[34,54,55] The dynamic yield stress (τ_d^0) is defined as the minimum stress required for maintaining the flow, while static yield stress (τ_s^0) is defined as the stress required for initiating flow, and the latter often has the higher value.[27,28,38] In this work we present the apparent yield stress of suspensions obtained using two different methods, shear flow measurements and oscillatory measurements. Shear flow measurements provide values of dynamic stress (τ_d) as a function of shear rate ($\gamma^{\bullet}$) and dynamic yield point (τ_d^0) while oscillatory strain steep measurements that provide values of static stress (τ_s) as a function of strain (γ) and thus enable defining of static yield point (τ_s^0), as the stress required for initiating of flow.[14,31,32,39] The Herschel–Bulkley equation describes the presence of a dynamic yield stress (τ_d^0) as

$$\tau_d=\tau_d^0+k\dot{\gamma}^n \quad (5)$$

where the terms k and n are the consistency and flow index, respectively. With the value of $n<1$ the material exhibits shear thinning, and for $n=1$ Newtonian behavior. For the determination of τ_d^0 a log–log plot of the flow curves were used, where the stress plateau at low shear rate is taken for each rheograms as a yield point stress (τ_d^0).[54]

Fitting the flow curve data to a yield stress model, however, can lead to a misconception of the yield stress determination, especially with rheologically complex thixotropic gel-like suspensions, in which the maintenance of flow is much less energy demanding than the initiation of flow because of the normally very long time constant of reestablishment of the gel structure.[26,27,29,36,47] Therefore, as in the case of MNFC complex suspensions, which also have properties of gels, it is preferable to determine yield stress values also by direct measurement with oscillatory experiments.[27,56] The elastic stress component in oscillatory mode is given by

$$\tau_s=G'\gamma \quad (6)$$

As strain (γ) is constantly increased at constant frequency (ω) from oscillatory amplitude sweep measurements, the maximum elastic stress, corresponding to the static elastic yield stress (τ_s^0), is determined as the first point of deviation from linear elastic deformation. The static yield stress occurs at a corresponding strain value (γ_c). The flow coefficient k and power law coefficient n from dynamic stress flow curves are obtained by linearization of the shear stress ($\tau-\tau_d^0$) against shear rate ($\gamma^{\bullet}$) log–log curves for $\gamma^{\bullet}>0.1\ s^{-1}$.[36,56] The flow coefficient $k^{\star}$ and power law coefficient $n^{\star}$ from static stress flow curves (within the linear viscoelastic region (LVE) are obtained from the log–log curves of complex viscosity (η^*) against angular frequency (ω).

Structure Recovery Measurements

The structure recovery measurements are made with the three interval thixotropic test (3ITT), the purpose of which is to determine how consistency, and the presence of a large amount of pigment accompanied with fibers, might lead to induced flocculation/agglomeration within the gel-like MFC matrix and so affect recovery of network structure after removal of high shear.[40,41] 3ITT measurement can be expected to provide information on the dynamic elastic structure recovery of MFC containing furnish after high shear deformation, say, in a head box and/or during fluidization. It is desirable that the initially high dynamic viscosity of MFC can be reduced at the head box slit and during application on a wire, in order to be in a reduced viscosity "flowing state" for application, and then to recover when forming the fiber mat.[5,13] Initially, in the first low shear interval, samples were subjected to low shear rate ($0.1\ s^{-1}$), then subsequently high shear rate ($500\ s^{-1}$) and finally once again low shear rate "recovery" ($0.1\ s^{-1}$). Structure recovery was traced with respect to recovery of dynamic transient viscosity (η^+) in the third interval, expressed as percentage (%) of ratio η^+/η^0 after 300 s of measurements, where η^0 is the low shear viscosity value at the beginning of the first interval.[5,41]

Dynamic Dewatering

Dynamic dewatering measurement was conducted using the same Physica MCR 300 rheometer with an immobilization cell (IMC) accessory, as licensed from BASF AG. The IMC consists of a stainless steel cylindrical metal tube with a hole-punched metal plate at its base that allows drainage of water through the samples.[42,43] A filter is fastened on the top of the metal plate, and the sample to be investigated is loaded into the cylindrical vessel. A parallel plate geometry measuring system (PP-50) with a 50 mm diameter was used in all immobilization tests, and initial gap was set to 2 mm.[24,25] The sample is dewatered through a Whatman nucleopore membrane, with pore size of 0.2 μm, by an applied vacuum of 50 kPa, which can be independently initiated (similar conditions to those in ÅA-GWR dewatering). The samples were presheared in the dynamic strain oscillation (DSO) cycle for 40 s, with oscillatory parameters, within the LVE, of $\gamma=0.1\%$ and $\omega=0.1$ (rad)s^{-1}, and then dewatering is allowed to proceed. Immobilization time (t_{imm}) of MFC containing furnishes were defined as the first minimum in the tan δ curves,

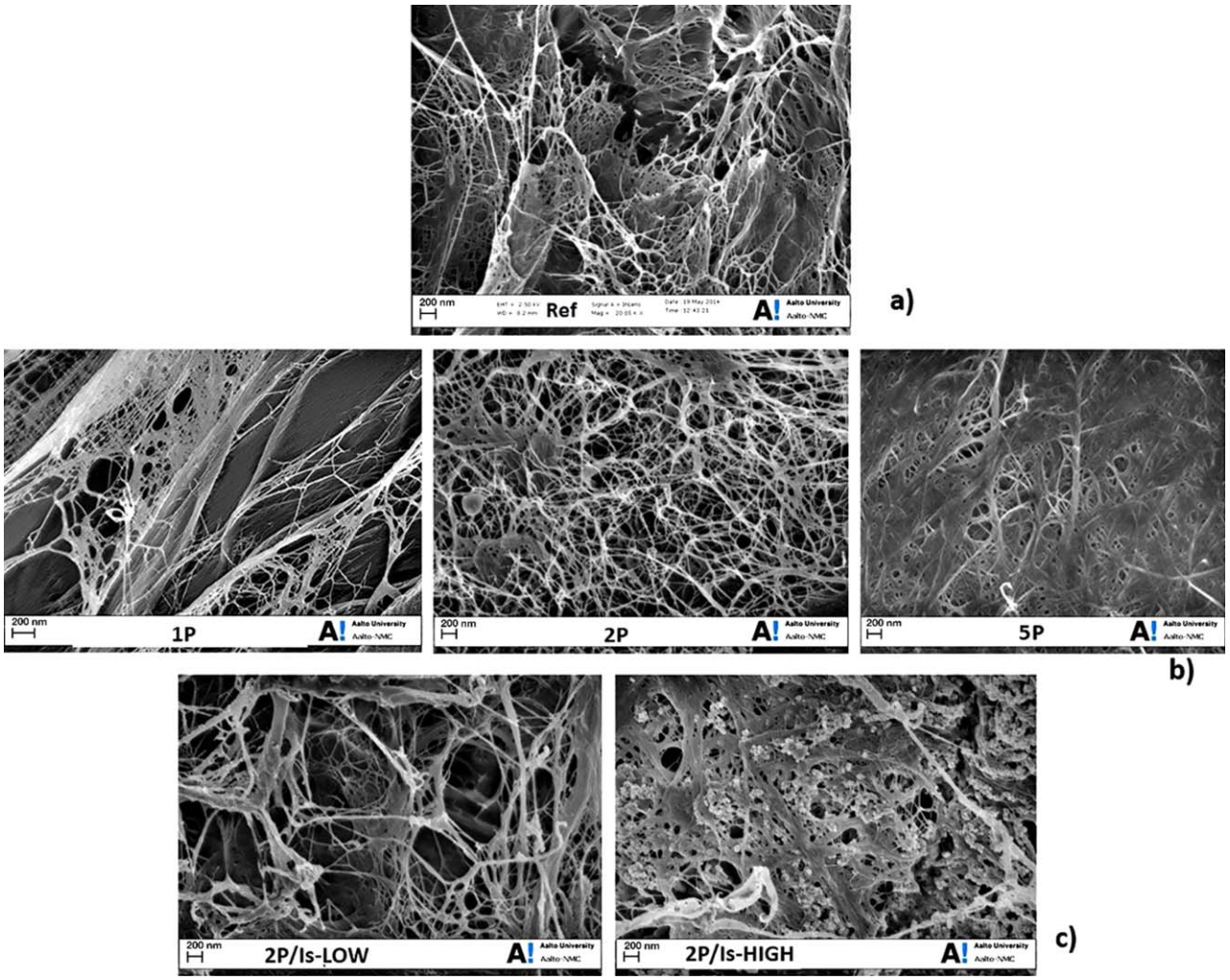

Figure 2. SEM images from **e**nzymatically treated MFC fibrils of different generation (scale bar 200 nm): (a) enzymatically pretreated and refined samples (Ref), (b) fluidized MFC fibrils from 1 pass (1P), 2 pass (2P) and 5 pass (5P), and (c) dispersed fibrils from 2 passes (2P) which have precipitated PCC filler on their surface, with 10.6% (LOW) and 75.5% (HIGH) filler precipitated on fibrils (Figure 1 and Table I). [Color figure can be viewed in the online issue, which is available at wileyonlinelibrary.com.]

where tan $\delta = G''/G'$, i.e. as the ratio between the loss and storage moduli in the viscoelastic region, as explained in our previous publication,[25] which also previously was shown to correspond to immobilization obtained by the intersection of the tangents of the two branches of the G' plots before and after yield.[42,44]

RESULTS AND DISCUSSION

We split the analysis into three sections. The first deals with the rheological transition from an entangled/flocculated structure to that of a gel-like structure driven by the fluidizing of the MFC component. By providing *in situ* precipitation of PCC filler onto the surface of the MFC component, the reduction of the contribution from the structure component can also be advanced. The second part deals with the response to shear for these different viscoelastic systems and highlights the critical stress factors applying in each. Finally, the third part links the findings of the previous two to elucidate the processes at play in the dewatering and immobilization of the suspensions.

The rheology of MFC suspensions is known to be dependent on the fines contained in the fibrillated cellulose, associated with surface charge and fibril morphology, which is expected to influence furnish rheology because of different friction and mobility properties within the furnish–filler matrix.[5,6,8,45] Therefore, it is important to evaluate in which way the increasing amount of passes through the fluidizer will change the fibril morphology, swelling of fibrils and suspension rheology. In this respect, one of the targets of this study was to examine the role of the fluidizing refining steps on enzymatically pretreated pulp on both particle and network swelling/gelation of MFC suspension. Optical microscopy, Figure 2, was used to facilitate the observation of disintegration of the enzymatically pretreated and refined fibrils into nano and microscale fibrils, and to demonstrate the importance of the fluidization in further fibrillation. The morphology of the resulting nanoscale fibrils after the enzymatic and mechanical treatment, Figure 2(a), has changed after the high pressure homogenization steps (1 pass, 2 pass, and 5 pass, respectively), Figure 2(b).

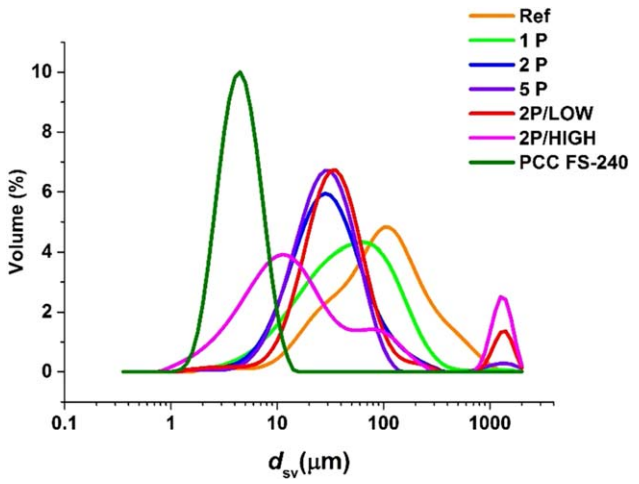

Figure 3. Fibrillated MFC agglomerates and PCC size distributions obtained using dynamic light scattering (DLS). As homogenizing degree progresses, the size distribution is seen to move to smaller values. [Color figure can be viewed in the online issue, which is available at wileyonlinelibrary.com.]

To be able to utilize properties of high aspect ratio cellulose nanofibrils fully, the dispersion with filler within the furnish matrix is critical. An improved dispersion of nano or microcellulosic components and filler is targeted by precipitation of filler onto the nano/microcellulose fibrils themselves, Figure 2(c), with two different flow rates of CO_2 prior to precipitation in the reactor, Figure 1, which resulted in two different *in situ* PCC-MFC composite costructures, *in situ*-LOW and *in situ*-HIGH, as presented in Table I.

A thorough description of the swelling of a fibrillar cellulose gel should include both the water trapped within the fibrillar network and the water immobilized inside and on the surface of the particles.[6,24,25] As presented in Figure 3(a), the water retention value (WRV) data demonstrate the greater water trapping nature of the more fibrillated 5 pass MFC (5MFC), where the number of passes influences the water arresting properties within the suspension matrix, increasing the MFC gel-network. Because of the effective size of the components, i.e., water surrounded MNFC versus non-water-interacting PCC, 2P/LOW and 2P/HIGH samples have lower median particle size than 2P, Table II.

The results from the WRV data, presented in Table II reflect the increase in water retention with increase in the number passes through the homogenizer. Samples 5P have evidently higher WRV than 2P and 1P. In contrast, as discussed earlier, reduction in the surface area of MNFC when pigment is precipitated on the fibril surface reduces swelling and water binding properties of the suspension, as discussed in our previous publication,[6] which is evident as a decrease in agglomerate size, Figure 3, showing a direct correlation of particle level swelling and network gel forming as a function of the increasing number of passes.

Viscoelastic Properties: The Structure–Gel Transition

Any differences in the degree of entanglement, agglomeration and/or flocculation in the network structure, resulting from the increased degree of fibrillation, should manifest itself in a change of mechanical and viscoelastic properties, including gelation. At the beginning of the strain sweep, with low strain (γ), both storage and loss moduli exhibit a constant value, G_0' and G_0'', respectively, with $G_0' > G_0''$ until a critical strain amplitude γ_c is reached, which defines the end of the linear viscoelastic region (LVE).[9,26,45,46]

The present high elastic moduli, Figure 4(a), seen with respect to the current reference and single fluidizing pass materials are explained by the presence of retained long fibrils and fibril agglomerates forming an inherently entangled network structure, which is not as evident for the more swollen higher fibrillated gel-like structure of the higher energy homogenized materials.[10,35,47]

The reduced form of the elastic (G'/G_0') and viscous moduli (G''/G_0''), presented in Figure 4(a,b), show the gelation effect of increasing homogenizing energy input and the reduction of the structure effect in nonhomogenized and once homogenized MFC containing furnish. As previously discussed, proceeding in homogenizing steps acts to fibrillate MFC further, producing

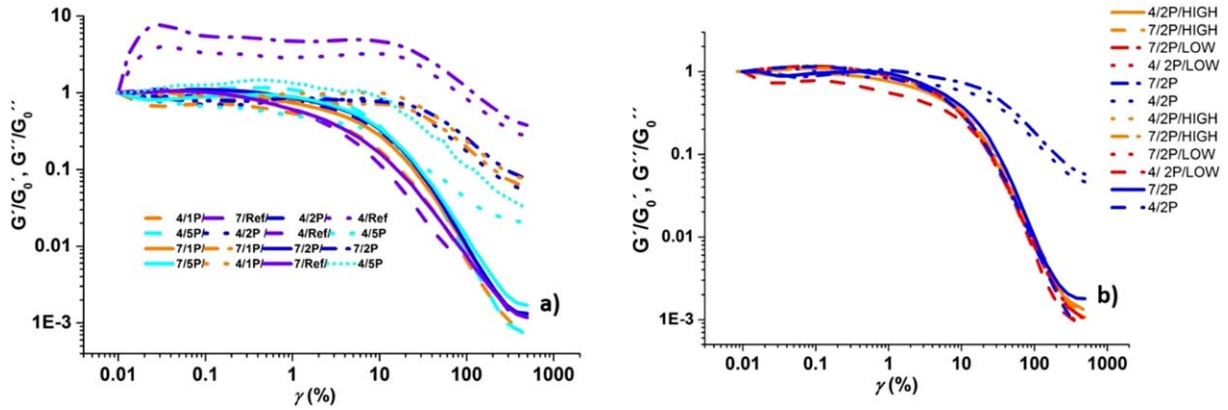

Figure 4. Reduced G' and G'' for furnishes in an amplitude sweep test for 4% and 7% consistencies: (a) reduced elastic (G'/G_0') and storage moduli (G''/G_0'') for different homogenization passes of MFC, (b) elastic moduli for 2MFC furnishes regarding the type of filler (*in situ* vs. mixing with suspension matrix): reduced elastic modulus (G'/G_0') shown as continuous lines, reduced loss modulus (G''/G_0'') as broken lines. [Color figure can be viewed in the online issue, which is available at wileyonlinelibrary.com.]

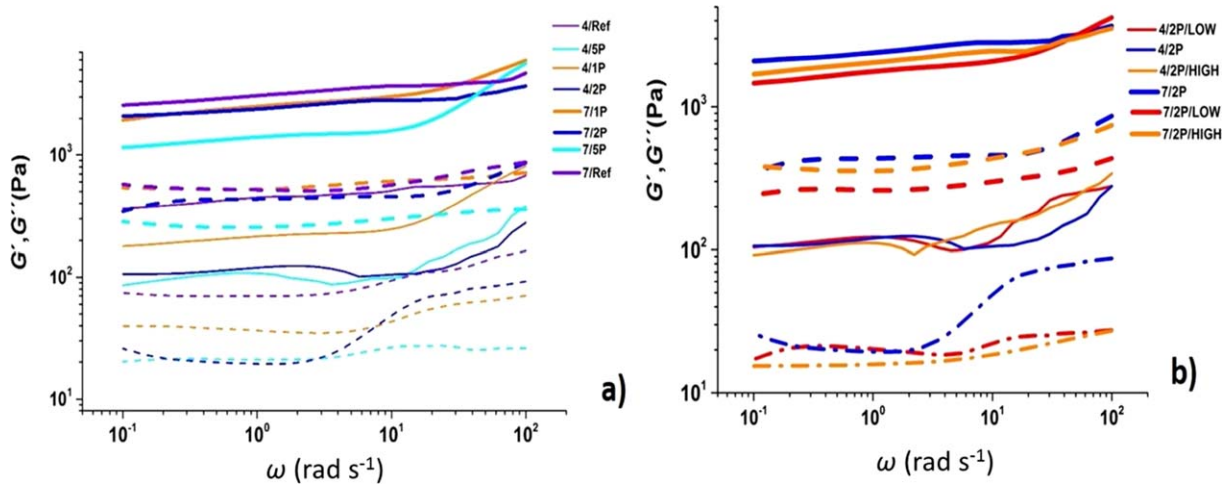

Figure 5. Response of G' and G' against frequency [$\omega = 0.1$–100 (rad)s^{-1}] for all furnishes at 4% and 7% consistencies, respectively: (a) furnishes for which 70% of pigment is added as separate inert component, Ref, 1, and 5 pass (1MFC, 5MFC), and (b) difference between *in situ* precipitation of filler and addition as separate component for 2 pass MFC (2P, 2P/HIGH and 2P/LOW, respectively): elastic modulus (G') shown as continuous lines, loss modulus (G') as broken lines. [Color figure can be viewed in the online issue, which is available at wileyonlinelibrary.com.]

finer fibrillar material with higher surface charge, thus increasing gelation of the suspension, which reduces flocculation within the furnish upon addition of inert filler and pulp fibers. Finer fibrillar material of the 5 pass MFC (5MFC) acts to reduce both the viscous (G') and elastic (G') moduli of the host furnish for both 4% and 7% consistency. When considering the effect of *in situ* precipitation of filler on 2MFC (*in situ* PCC-2MFC costructure), the greater the amount of precipitated filler onto the fibrillar cellulose, and in turn the lower the amount of filler added as separate inert component to the furnish, results in lower structuration induced by phase separation of gel-like MFC (inert filler and agglomerated pulp fibers).[41] This is seen as a decrease of both G' and G' as the amount of filler precipitated on the fibrils is increased. The data indicate that G' is dependent on consistency, as expected, and that, for the non-fluidized enzymatically pretreated reference MFC based furnishes, G' relates even more strongly to consistency than the homogenized samples, i.e. G' overall decreases with the number of passes through the fluidizer across all measured consistencies, and this despite the greater gelation tendency, which clearly separates the two structure mechanisms. This entanglement, therefore, relates inversely to the higher swelling-related WRV, and in turn higher zeta potential, which has been observed before.[9,41] As shown in the same Figure 4, once above critical strain (γ_c), G' decreases gradually with increasing strain (γ), while the loss moduli (G') exhibit a strain hardening characterized by an overshoot in the curve when strain is increased more rapidly than the equilibrium relaxation of the system.[45,46] Loss modulus increase, indicating strain hardening, is typical for agglomerated linear particulate gel systems incorporating the presence of fillers and their respective complex nature of interactions.[47–49] Loss moduli overshoots can also be observed, related to the nonlinear oscillatory response of gel-like materials undergoing shear banding and wall slip—a typical drawback when interpreting data from plate–plate geometry.[34,37,50]

It is known that for gel-like nanocellulose suspensions G' and G' are relatively independent of angular frequency.[11,27,47,50] The data in Figure 5(a,b) suggest a similar behavior of elastic moduli as a function of oscillation frequency as was discussed above in relation to Figure 4. High consistency furnishes are entangled/flocculated suspensions of cellulose macrofibers, microfibrillar material (MFC), and fillers.[42] Their rheological behavior is, therefore, expected to depend on the solids concentration and the interaction of all the components. This becomes manifest in the shear strain amplitude dependence of the storage modulus (G') and the viscous modulus (G') measured at the constant angular frequency $\omega = 0.1$ (rad) s^{-1}, for all furnishes. Progressive energy input by homogenizing, and thus related gelation within the fibrillar cellulose component, is reflected in the reduction in both G' and G' for the respective furnish mixes within the given angular frequency range (ω) Figure 5(a), acting in the same way as addition of filler through precipitation for the same homogenizing energy input Figure 5(b), as discussed above. Consistency dependence is seen through the range in gel-structure between the 4% and 7% furnishes as frequency increases, where G' and G' decrease for higher consistency furnishes, Figure 5(a), and for lower amount of pigment added as a separate component to the 2MFC containing furnish. Thus, for the 2 pass sample (2MFC), where the MFC is coated with nanoscale *in situ* formed PCC filler and the remaining filler amount is postmixed with the furnish, increasing the amount of *in situ* precipitated pigment shows a decrease in G' and thus less structuring within the furnish matrix. As can be seen in Figure 5, this effect is consistent with results shown in the previous Figure 4, where the G' for highly fibrillated cellulose containing furnishes are generally lower than those of less fibrillated MFC containing furnishes, as the more swollen the fibrillar material, the more pronounced the disentanglement and/or deflocculation within the furnish.[9,35,41] The G' is nearly independent of frequency, while the G' is constant

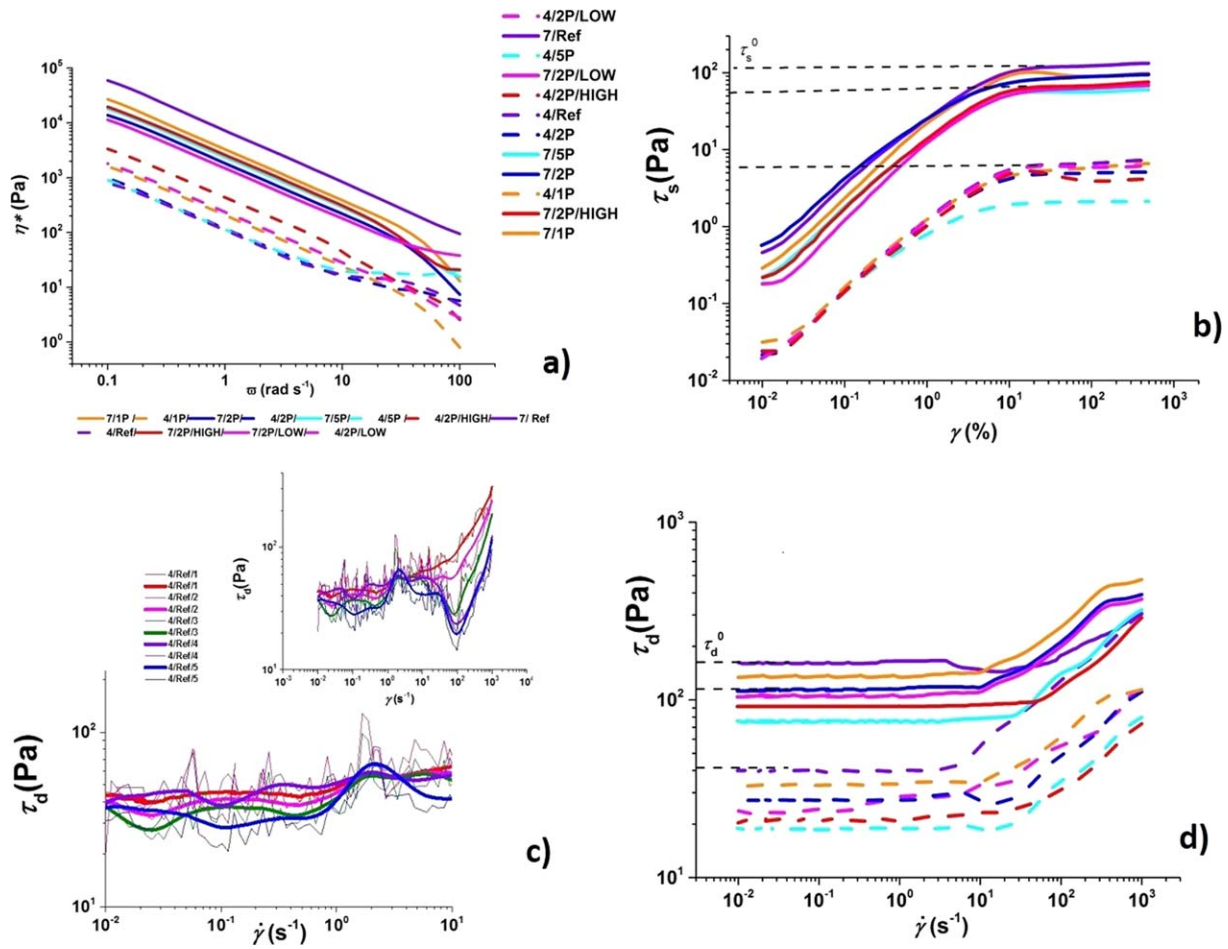

Figure 6. Oscillatory and dynamic rotational measurements: (a) complex viscosity as a function of frequency, (b) static stress (τ_s) within the LVE as a function of strain (γ), (c) dynamic stress (τ_d) as a function of shear rate for 4 Ref samples, raw data and smoothed data [eqs. (2)–(4)], and (d) representative samples of dynamic yield stress obtained at low shear rate, $\gamma^{\cdot} = 0.01$–$10\ s^{-1}$ [eq. (5)]. Broken lines 4% consistency and continuous lines 7% consistency. [Color figure can be viewed in the online issue, which is available at wileyonlinelibrary.com.]

at low frequency and increases slightly at higher frequencies, tan δ being in between 0.2 and 0.3. In other words, the more highly homogenized materials behave as weak gels.

The relative response of the furnishes regarding the degree of homogenizing, and the role of fibrillation, is seen in all the data as a progressive increase in gelation of the more highly fibrillated suspension matrix, and a reduction in the mechanical elasticity derived from the entangled fibril structure of less fluidized material.

Shear Thinning and Recovery Behavior

Being viscoelastic, the structure of the agglomerated/flocculated network changes when it is sheared.[9,27,47,57] The plots in Figure 6(a) show the η^* decrease as a function of increasing $\omega = 0.1$–100 (rad) s^{-1} within the LVE region, and corresponding static yield stress (τ_s^0) Figure 6(b) obtained using eq. (6). Complex rheological behavior in shearing conditions is presented in the steady state flow curves of furnishes at shear rates 0.1 – 1 000 s^{-1} in Figure 6(c,d), through dynamic stress (τ_d) dependence on shear rate ($\gamma^{\cdot}$), eq. (5). We illustrate both the raw data and the smoothed resulting curves for the sampling of 4 Ref (4% consistency), Figure 6(c), to illustrate the complex rheological response under shearing conditions. The data are shown with respect to stress only in Figure 6(c).[9,10,57]

The static (τ_s^0) and dynamic yield stress (τ_d^0) of all furnishes increases with consistency, Table III. Flow curves with fitted power law exponents for both dynamic viscosity (η) and complex viscosity (η^*) vary between 0.14 and 0.11, in agreement with some examples of earlier work with MNFC suspensions[26] and furnishes.[27] Increase in consistency and greater flocculation tendency within the complex suspension matrix are seen in a higher k value, while very pronounced shear thinning behavior is because of the breakdown response of the highly viscoelastic gel-like structure to shear.[24–29]

In Figure 6(c), the higher consistency furnishes show the greater τ_e as a function of strain (γ), as might be expected. Similar behavior is observed for τ as a function of shear rate ($\gamma^{\cdot}$), Figure 6(d). The structuration[41] within the furnish matrix increases the span of both τ_e and τ, as the mechanical agglomeration/flocculation of entrapped water within the gel increases the stress response of the material.[26,38,46] This behavior is, thus, as described above, consistency dependent and the mechanical structure factor is reduced by increased homogenizing energy

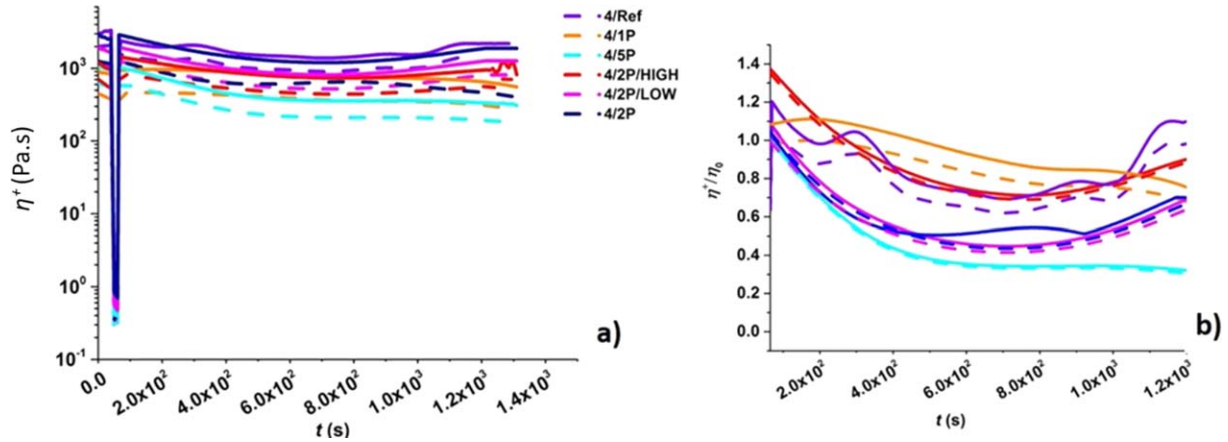

Figure 7. Viscosity as a function of time illustrating structure recovery obtained from the 3ITT procedure: (a) transient viscosity (η^+) in the three intervals in the low/high/low shear regime, and (b) 3ITT curves for all furnishes with structure recovery expressed as reduced value of η^+ with η_0, where η_0 is the initial dynamic viscosity in the first low shear interval. Open lines 4% consistency and closed lines 7% consistency. [Color figure can be viewed in the online issue, which is available at wileyonlinelibrary.com.]

input, because of the transition to a more gel-like response. A similar effect is seen when *in situ* PCC is formed on the 2 pass MFC (is-situ PCC-2MFC costructure), i.e., agglomerate forming structuration is reduced. We can conclude that this is semiindependent of the PCC filler added separately, since the homogenizing energy input of the MFC component follows this behavior of reduction in structuration, even whilst the free-added PCC level remains high in the system, reflected in the development of τ_s^0 in Figure 6(c), and τ_d^0 in Figure 6(d). This manifests the long range interaction of the MFC fibrillar length compared with shorter higher charged nano only fibrils (NFC), which is approached by the highly fluidized MFC,[6,19] which in turn could be better described as MNFC. Scatter in the data between yield stress obtained by oscillation and steady shear measurements has been observed before,[31,33,35,50] and depends on how apparent yield stress is defined and the method of measurement employed.[9,27,52] The apparent yield stress of all furnishes increases with consistency, which compares typically with other research done on similar subject materials; differences in τ_s^0 and $\tau_d{}^0$ between different furnish types are small at low solids content, but more pronounced for the higher solids content.[26]

An important conclusion regarding the structure recovery after high shear, Figure 7, is that the transient dynamic viscosity recovery (η^+) after high shear is a slow process, especially for the highly homogenized MFC containing furnish samples, resulting from breakage of the fibrillar gel-like structure and its subsequent slow diffusion controlled reformation. This informs us that a suspension takes a long time to recover its structure if the MFC component has been highly fibrillated, resulting in good levelling behavior, for example, after initial dewatering following the rapid shear increase at the slide prior to the forming section.[5,41,45]

Dewatering and Immobilization

Dynamic Dewatering IMC. The immobilization curves of the various MFC containing furnishes are characterized by an increase in complex viscosity, which indicates faster initial dewatering and steeper increase in solids for furnishes with more agglomerated/entangled/flocculated structure and lower MFC network swelling.[25,41] This confirms the more permeable nature and lack of water trapping properties within the mechanical interfibrillar formed structure. After the initial increase in η^*, G', and tan δ, Figure 8(a,b) related to the first stage dewatering, both η^* and G' reach a plateau, the value of which depends on the amount of water entrapped in the gel structure. The progressive increase of tan δ shows different time scales in which the maximum of tan δ is reached, Figure 8(c). In the case of more gel-like structures, defined by the amount of refining by homogenizing, the timescale is longer. Interestingly, for the *in situ* precipitated PCC on MFC (*in situ* PCC-2MFC costructure), the uniformity of the matrix (without entanglement/flocculation) matches that of the higher energy input homogenized sample, but the dewatering rate is fast, indicating that the *in situ* precipitation of PCC onto the MFC reduces the gel trapping of water, whilst nonetheless preventing the particle structural flow problems associated with the nonhomogenized or low energy homogenized samples. As discussed in our previous research, it is not possible to define final immobilization time as a fixed point at which tan δ reaches a plateau, rather it is necessary to use turning points on the rheograms, or the minimum of the tan δ curve, defined also by the second zero of $d\tan\delta/dt$, as indicating complete immobilization.[24] Because of the wide-ranging nature of the rheograms upon increase of consistency, representative samples are considered with respect to an "application representative" definition, i.e. samples lying within a range of potential application in the field studied by the paper.

Data presented in Figure 8(c) show the change in tan δ, indicating similar dependence on consistency for the time taken to the onset of immobilization t_{imm}, but differences are observed between mechanical entanglement/structuration within the furnish matrix, as the lower the degree of swelling, so the lower is the WRV and the greater the dewatering. The value of tan δ characterizes the viscoelasticity of the material as a ratio of the viscous loss and elastic storage moduli, G'/G',[57] marking the transition of liquidlike to solidlike behavior during dewatering.[43]

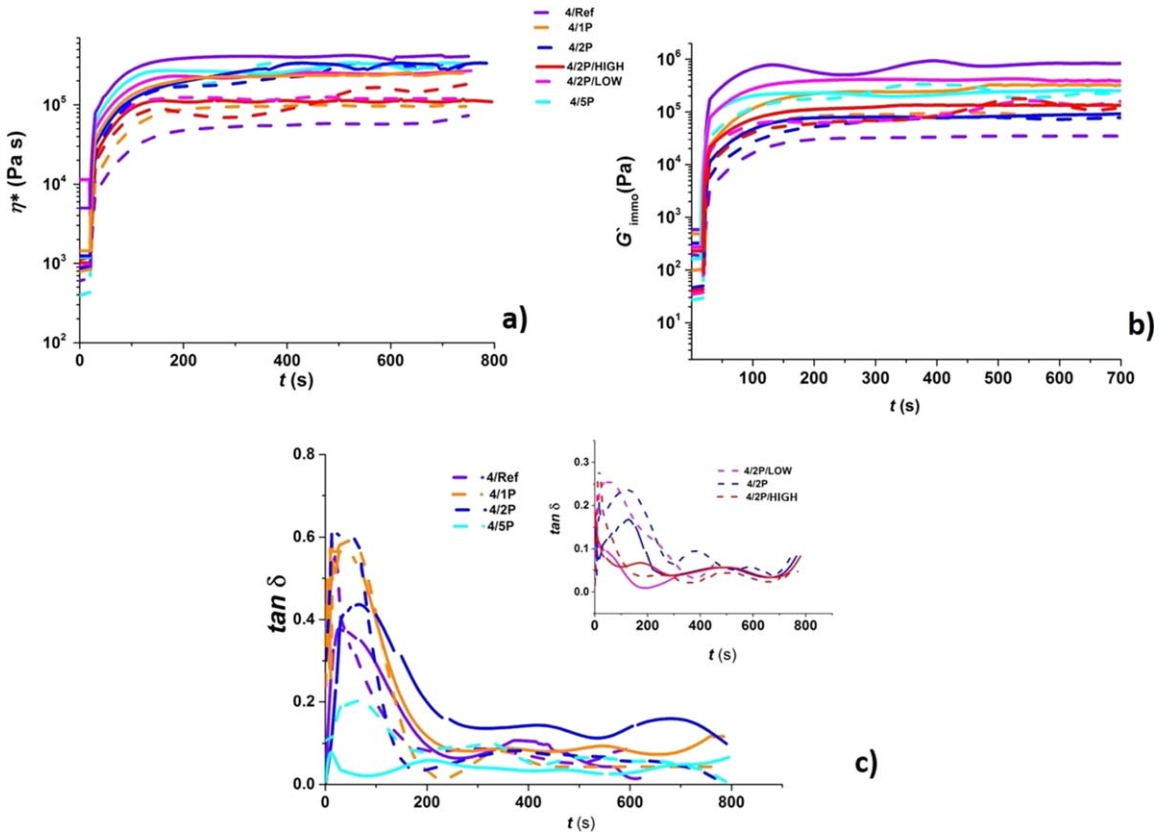

Figure 8. Immobilization rheograms for all furnishes: (a) elastic modulus (G'), (b) complex viscosity η^*, and (c) damping factor (tan δ) showing progress toward immobilization. The wavy nature of the curves suggests nonequilibrium regions of dewatering probably induced by shear banding and wall slip under the intermediate shear regime: broken lines 4% consistency and continuous lines 7% consistency. [Color figure can be viewed in the online issue, which is available at wileyonlinelibrary.com.]

Gravimetric Dewatering (ÅA-GWR)

In this section we compare the static pressure dewatering (water retention) using the ÅA-GWR device with the dynamic immobilization under shear, Figure 9. The more uniform dispersion of components in the furnish matrix that contains *in situ* precipitated filler on the surface of MFC, i.e., *in situ* PCC 2MFC costructure (2P/LOW and 2P/HIGH), indicates that the pigment distributed on the MFC surface acts to reduce the action of trapping water, as was presented in Figure 8, leading to greater mobility of water within the matrix, which results in faster

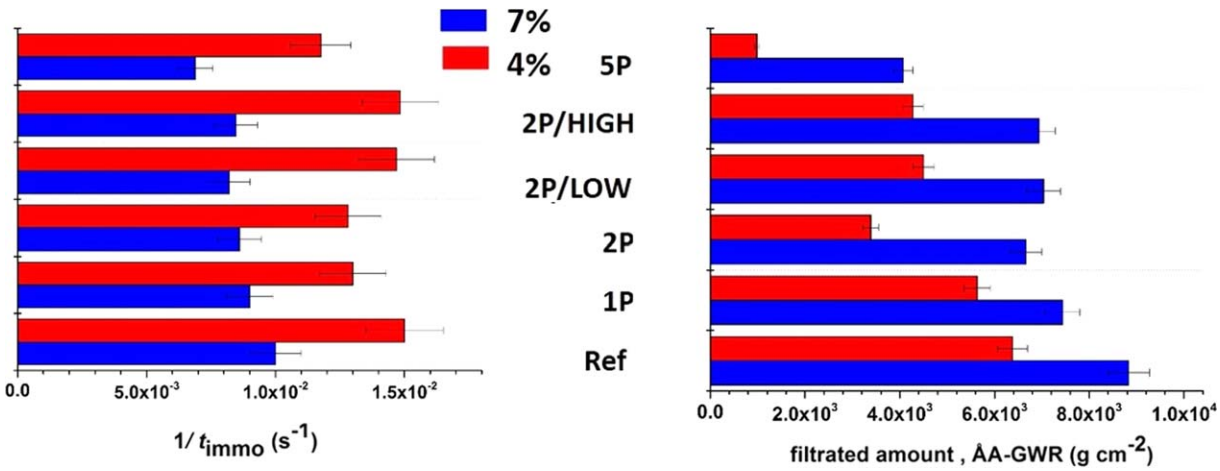

Figure 9. Correlation amongst furnishes between filtrate amount with ÅA-GWR and immobilization time (t_{imm}) against furnish type showing dependence of agglomeration within the furnish matrix and dewatering. [Color figure can be viewed in the online issue, which is available at wileyonlinelibrary.com.]

Table II. WRV, Surface Charge ζ, pH and Median Size of MFC Agglomerates and PCC used in the Study

	WRV (gg^{-1})	ζ (Mv)	pH	*d* (0.5) (μm)
Ref	1.5	−26.4	6.8	89.4
1P	2.8	−22.1	6.7	43.7
2P	3.7	−25.5	6.7	29.1
2P/LOW	2.1	−12.3	9.2	14.9
2P/HIGH	1.8	−12.7	10.3	14.2
5P	5.1	−30.8	6.8	28.3
freely added PCC/FS-240	N.A.	10.6	10.3	4.1

dewatering. The dynamic immobilization rate results correlate with gravimetric dewatering and confirm that the intrinsic structure is less water retaining rather than that the structure is more easily broken down under shear.[24,25]

Linking All Aspects of the Rheological and Dewatering Observations

In order to compare the different response of complex (η^*) and dynamic (η) viscosities we use iterative least squares methods to reveal values of their flow coefficients, together with the respective fitted values for shear thinning index *n*, respectively, as in eq. (5). We see in most cases that *k* is larger for the more agglomerated furnishes that contain the less fibrillated MFC, indicating lower mobility of the longer fibril elements, i.e. more entanglement, and greater phase separation between the long cellulose fibers and pigment. This observation is also valid when considering the reduced agglomeration/flocculation for the *in situ* PCC-2MFC costructure containing furnish, in which part of the pigment is precipitated on the MFC. That the agglomerated structuration is occurring to a lesser degree in this *in situ* PCC case, even in the presence of more fluidized 2MFC, supports the dominance of gel formation and absence of floc-related structures involving pigment, which, if it were to be flocculated by the gel component, would lead to less homogeneous low elasticity initial flow, and clearly this is not occurring. Also, that the more refined MFC containing system, which also has pigment added as a separate phase (not *in situ* precipitated), is not (or less) flocculated suggests that it is supported in stable suspension by the greater repulsion at higher charge level zeta potential of the more fluidized MFC, and that the pigment is an inert player in the suspension mix. This finding is supported by previous work studying the flow properties of pigmented coating colors employing MNFC, dispersed additionally with carboxymethyl cellulose (CMC).[41]

Table III contains a summary of the collected data and their parameterization, providing comparison of the effective rheological behavior obtained from oscillatory and steady state studies, together with immobilization during dewatering and structure recovery after shear. Average values of G' and G' obtained at 0.16 $(rad)s^{-1}$ for all furnishes further confirm the previous interpretation that the G' for the nonhomogenized MFC containing furnishes is higher compared to the more fibrillated ones. Higher WRV implies greater swelling and thus lower friction of the highly fibrillated cellulose as seen in lower G'. In general, the yield stress (τ_s^0 and τ_d^0) of the structured suspension depends on the solids content, particle size distribution and particle–particle interactions defined from Table II.[47,53] The apparent τ_c for all furnishes is a function of consistency, as plotted in Figure 7.

CONCLUSIONS

This study undertakes to represent the changes in the rheological and dewatering properties of MNFC when the level of fibrillation increases, and when used as a component in fiber and filler composite furnish. It is seen that this transition occurs in two major observable forms: (i) the water retention properties increase as the transition progresses toward the gel, related to the water binding and interparticulate trapping in highly fibrillated MFC, more correctly termed in this state as MNFC, and (ii) the reduction of fibrillar entanglement as this transition progresses leading to reduced viscoelasticity and slower structure recovery after shear.

Table III. Static Yield Stress (τ_s^0) Obtained from Oscillatory Measurements within the LVE Region, Using eq. (6), and Dynamic Yield Stress (τ_d^0) Obtained from Dynamic Measurements Using eq. (5)

	4/REF	4/1P	4/2P	4/2P/ LOW	4/2P/ HIGH	4/5P	7/REF	7/1P	7/2P	7/2P/ LOW	7/2P/ HIGH	7/5P
k	16.6	19.7	62.2	55.4	43.6	40.4	44.6	92.1	83.1	68.6	78.4	65.2
n	0.21	0.16	0.11	0.13	0.17	0.08	0.16	0.15	0.10	0.11	0.12	0.09
k^*	18.2	21.7	69.2	58.3	47.3	12.3	57.2	96.1	86.2	71.1	80.3	57.2
n^*	0.21	0.17	0.14	0.11	0.13	0.09	0.18	0.15	0.16	0.13	0.14	0.09
τ_s^0 (Pa)	6.4	6.4	4.5	5.2	5.8	2.5	119.2	99.9	82.3	64.2	62.3	57.4
τ_d^0 (Pa)	38.2	32.7	27.4	20.7	18.9	16.4	162.9	133.9	114.2	103.6	91.7	75.9

Shear thinning behavior for all furnishes: initial and final values of flow curves for complex viscosity response (η^*) and dynamic viscosity (η) with their respective flow indexes (*k*, k^*) and shear thinning coefficients (*n*, n^*). Data variation for rheological measurements are within ± 10% because of the thixotropic and wall slip phenomena arising from the complex nature of MNFC suspensions

A novel costructure, consisting of calcium carbonate precipitated *in situ* on the surface of a moderately homogenized MFC, provides advantageous properties in the furnish with respect to enhanced dewatering whilst maintaining the flow properties of a gel-like state. These changes in the traditional water retention properties of microfibrillated cellulose are expected to lead to improved sheet forming properties, with increased water removal, and so lower drying cost, and controlled uniform settling during subsequent recovery after shear. These properties are expected also to lead to more uniform filler-fiber composite materials in the advancing field of cellulosic composite production.

REFERENCES

1. Hassan, E. A.; Hassan, M. L.; Oksman, K. *Wood Fiber Sci.* **2011**, *43*, 76.
2. Duncan, T. V. *J. Colloid Interface Sci.* **2011**, *1*, 1.
3. Pääkkö, M.; Vapaavuori, J.; Silvennoinen, R.; Kosonen, H.; Ankerfors, M.; Lindström, T.; Berglund, L. A.; Ikkala, O. *Soft Matter* **2011**, *4*, 2492.
4. Kajanto, I.; Kosonen, M. *J-for-J. Sci. Technol. Forest Prod. Process.* **2012**, *2*, 42.
5. Rantanen, J.; Dimic-Misic, K.; Pirttiniemi, J.; Kuosmanen, P.; Maloney, T. C. *BioResearch* **2015**, *10*, 3492.
6. Rantanen, J.; Dimic-Misic, K.; Kuusisto, J.; Maloney, T. C. *Cellulose* **2015**, DOI: 10.1007/s10570-015-0777-x.
7. Turbak, A. F.; Snyder, F. W.; Sandberg, K. R. Nonwovens Symposium, Myrtle Beach, SC, Apr. 16–19, **1984**, pp 115.
8. Subramanian, R.; Hiltunen, E.; Gane, P. A. C. Cellulose Fibers, Bio-and Nano-Polymer Composites: Green Chemistry and Technology; Springer Verlag: Berlin, **2011**; Part II, Chapter 5, pp 121
9. Horvath, A. E.; Lindström, T. *J. Colloid Interface Sci.* **2007**, *309*, 511.
10. Saarikoski, E.; Saarinen, T.; Salmela, J.; Seppälä, J. *Cellulose* **2012**, *19*, 647.
11. Iotti, M.; Gregersen, ØW.; Moe, S.; Lenes, M. *J. Polym. Environ.* **2011**, *19*, 137.
12. Hii, C.; Gregersen, ØW.; Chinga-Carrasco, G.; Eriksen, Ø. *Nordic Pulp Paper Res. J.* **2012**, *27*, 388.
13. Spence, K. L.; Venditti, R. A.; Rojas, O. J.; Habibi, Y.; Pawlak, J. *J. Cellulose* **2011**, *18*, 1097.
14. Bennington, C. P. J.; Kerekes, R. J.; Grace, J. R. *Can. J. Chem. Eng.* **1991**, *69*, 251.
15. Herrick, F. W.; Casebier, R. L.; Hamilton, J. K.; Sandberg, K. R. Journal of Applied Polymer Science, **1983**, Applied Polymer Symposium, 37, conf. 8205294
16. Klemm, D.; Kramer, F.; Moritz, S.; Lindström, T.; Ankerfors, M.; Gray, D.; Dorris, A. *Angew. Chem. Int. Ed.* **2011**, *50*, 5438.
17. Saito, T.; Isogai, A. *Biomacromolecules* **2004**, *5*, 1983.
18. Pääkkö, M.; Ankerfors, M.; Kosonen, H.; Nykänen, A.; Ahola, S.; Österberg, M.; Lindström, T.; Ruokalainen, J.; Laine, J.; Larsson, T. *Biomacromolecules* **2007**, *8*, 1934.
19. Henriksson, M.; Henriksson, G.; Berglund, L. A.; Lindström, T. *Eur. Polym. J.* **2007**, *4343*, 3434.
20. Janardhnan, S.; Sain, M. M. *Bioresources* **2007**, *1*, 176.
21. Nakagaito, A.; Yano, H. *Appl. Phys. A* **2004**, *78*, 547.
22. Andresen, M.; Stenius, P. *J. Disper. Sci. Technol.* **2007**, *28*, 837.
23. Eriksen, O.; Syverud, K.; Gregersen, O. *Nordic Pulp Paper Res. J.* **2008**, *23*, 299.
24. Dimic-Misic, K.; Puisto, A.; Paltakari, J.; Alava, M.; Maloney, T. *Cellulose* **2013**, *20*, 1853.
25. Dimic-Misic, K.; Puisto, A.; Gane, P.; Nieminen, K.; Alava, M.; Paltakari, J.; Maloney, T. *Cellulose* **2013**, *20*, 2847.
26. Lasseuguette, E.; Roux, D.; Nishiyama, Y. *Cellulose* **2008**, *15*, 425.
27. Richmond, F.; Co, A.; Bousfield, D. Proc., Paper Conference and Trade show, PaperCon **2012**, p 662.
28. Fall, A. B.; Lindströ, m.; Sundman, S. B.; odberg, O.; Wa˚gberg, L. L. *Langmuir* **2011**, *27*, 11332.
29. Puisto, A.; Illa, X.; Mohtaschemi, M.; Alava, M. *Nordic Pulp Paper Res. J.* **2012**, *27*, 277.
30. Dolz, M.; Bugaj, J.; Pellicer, J.; Hernández, M. J.; Górecki, M. *J. Pharm. Sci.* **1997**, *86*, 1283.
31. Barnes, H. A. *Appl. Rheol.* **2007**, *17*, 43110.
32. Buscall, R. *J. Rheol.* **2010**, *54*, 1177.
33. Bertola, V.; Bertrand, F.; Tabuteau, H.; Bonn, D.; Coussot, P. *J. Rheol.* **2003**, *47*, 1211.
34. Møller, P. C. F.; Mewis, J.; Bonn, D. *Soft Matter* **2006**, *2*, 274.
35. Mohtaschemi, M.; Dimic-Misic, K.; Puisto, A.; Korhonen, M.; Maloney, T.; Paltakari, J.; Alava, M. *J. Cellulose* **2014**, *21*, 1305.
36. Divoux, T.; Tamarii, D.; Barentin, C.; Manneville, S. *Phys. Rev. Lett.* **2010**, *104*, 208301.
37. Ovarlez, G.; Rodts, S.; Chateau, X.; Coussot, P. *Rheol. Acta* **2009**, *48*, 831.
38. Derakhshandeh, B.; Kerekes, R. J.; Hatzikiriakos, S. G.; Bennington, C. P. *J. Chem. Eng. Sci.* **2011**, *66*, 3460.
39. Boger, D. V.; Hur, D. U.; Binnington, R. J. *J. Nonnewton. Fluid Mech.* **1986**, *20*, 31.
40. Deka, A.; Dey, N. *J. Coat. Technol. Res.* **2013**, *10*, 305.
41. Dimic-Misic, K.; Gane, P. A. C.; Paltakari, J. *Ind. Eng. Chem. Res.* **2013**, *52*, 16066.
42. Wollny, K. *Appl. Rheol.* **2001**, *11*, 197.
43. Willenbacher, N.; Hanciogullari, H.; Radle, M. *Tappi J.* **1999**, *82*, 167.
44. Ayol, A.; Dentel, S. K.; Filibeli, A. *J. Rheol.* **2007**, *51*, 1253.
45. Rantanen, J.; Lahtinen, P.; Maloney, T. *Int. Paperworld IPW* **2015**, *5*, 46.
46. Klein, C. O.; Spiess, H. W.; Calin, A.; Balan, C.; Wilhelm, M. *Macromolecules* **2007**, *40*, 4250.
47. Naderi, A.; Lindström, T.; Sundström, J. *Cellulose* **2014**, *21*, 1561.

48. Karppinen, A.; Vesterinen, A.; Saarinen, T.; Pietikäinen, P.; Seppälä, J. *Cellulose* **2011**, *18*, 1381.
49. Whittle, M.; Dickinson, E. *J. Chem. Phys.* **1997**, *107*, 10191.
50. Ridgway, C. J.; Gane, P. A. C. *J. Pulp Paper Sci.* **2007**, *33*, 71.
51. Nechyporchuk, O.; Belgacem, M. N.; Pignon, F. *Cellulose* **2015**, 2197.
52. Björkman, U. *Appl. Rheol.* **2008**, *18*, 23974. 1
53. Dalpke, B.; Kerekes, R. *J. Pulp Paper Sci.* **2005**, *31*, 39.
54. Beghello, L.; Eklund, D. *J. Pulp Paper Sci* **1999**, *25*, 246.
55. Yang, M. C.; Scriven, L. E.; Macosko, C. W. *J. Rheol.* **1986**, *30*, 1015.
56. Lindström, T., Carlsson, G. Svensk Papperstindning-Nordisk Cellulosa, **1982**, *85*, 14
57. Pääkkönen, T.; Dimic-Misic, K.; Orelma, H.; Pönni, R.; Vuorinen, T.; Maloney, T. *Cellulose* **2015**, 1.
58. Dimic- Misic, K.; Nieminen, K.; Gane, P.; Maloney, T.; Sixta, H.; Paltakari, J. *Appl. Rheol.* **2014**, *24*, 35619.